Fluorenyl Zinc Phosphonate Zn(H 2 O)PO 3 -C 13 H 9 ×H 2 O: Hybrid Columnar Structure with Strong C-H×××π Interactions

Clarisse Bloyet, Jean-Michel Rueff, Vincent Caignaert, Jean-François Lohier, Julien Cardin, Paul-Alain Jaffres, Bernard Raveau

Fluorenyl Zinc Phosphonate $Zn(H_2O)PO_3$–$C_{13}H_9$·H_2O: Hybrid Columnar Structure with Strong C–H···π Interactions

Clarisse Bloyet,[a] Jean-Michel Rueff,[a] Vincent Caignaert,[a] Jean-François Lohier,[b] Julien Cardin,[c] Paul-Alain Jaffrès,[d] and Bernard Raveau*[a]

Dedicated to Professor Anthony K. Cheetham on the Occasion of his 70th Birthday

Abstract. A new zinc phosphonate $Zn(H_2O)PO_3$–$C_{13}H_9$·H_2O with a columnar structure was synthesized in hydrothermal conditions. This compound crystallizes in space group $P2_1/c$ [a = 15.832(4) Å, b = 5.1915(10) Å, c = 17.519(4) Å and β = 114.479(6)°]. Its inorganic framework consists of isolated chains of corner-sharing $ZnO_3(H_2O)$ and PO_3C tetrahedra. These chains are linked to fluorene cycles, forming hybrid columns, interconnected through C–H···π bonds. The photoluminescence properties of this hybrid material show that its emission bands are red shifted with respect to those of the mother phosphonic acid. This effect is explained on the basis of the structural constraints imposed by the inorganic Zn-phosphonate chains.

Introduction

Hybrid inorganic-organic materials with a framework consisting of conjugated aryl molecules associated with a transition d^{10} metal cation such as zinc or cadmium have a great potential for luminescence applications as illustrated by numerous coordination polymers with supramolecular structures and metal-organic frameworks (see[1–3] and references cited therein). In these d^{10} metal complexes, two structural features participate in the photo-luminescence (PL): the π–π stacking and the C–H···π interactions between the organic ligands on one side and the π···ns ligand-to-metal charge transfer (LMCT) on the other side. In this respect, transition metal phosphonates provide a potential source for the realization of luminescent materials since they can contain both d^{10} transition element and aryl ligands.

Metal phosphonates were reported for the first time almost forty years ago by *Alberti* et al.[4] opening the route to the discovery of hundreds of compounds with an extremely rich chemistry (see for a review[5–11]) and covering a wide range of applications, such as biotechnology, catalysis, gas storage, and photoluminescence.[7,12–15] In contrast, the number of zinc phosphonates containing conjugated molecules[16] or ligands,[17–24] which show PL properties is quite limited. These compounds are either phosphono-biphenyl carboxylates[17,18] or triazine-based phosphonates,[19] or contain terephthalate linkers,[20] naphthyl groups,[21] phenyl-sulfonyl groups[22] or pyrazine groups,[23] or even more simply benzyl groups.[24] The primordial role of the organic ligand, especially the π–π stacking,[25] and the C–H···π interactions in the PL properties of these phosphonates has been emphasized by most of the authors,[17–23] whereas in contrast the role of the $3d^{10}$ zinc cation is still not elucidated and requires further investigation as suggested for the phenyl phosphonate $Zn(O_3PC_6H_5)$·H_2O.[24]

Based on the above observations we believe that a systematic investigation of zinc phosphonates containing conjugated ligands should allow the PL properties of these materials to be understood and optimized in view of applications. In this paper, we present the synthesis and structure of a novel zinc phosphonate, $Zn(H_2O)PO_3$–$C_{13}H_9$·H_2O involving a fluorene ligand and we show that the PL emission peaks of this compound are red shifted with respect to the mother fluoren-9-yl-phosphonic acid.

* Prof. Dr. B. Raveau
E-Mail: Bernard.raveau@ensicaen.fr
[a] Normandie Univ, ENSICAEN, UNICAEN, CNRS, CRISMAT
14000 Caen, France
[b] Normandie Univ, ENSICAEN, UNICAEN, CNRS, LCMT
14000 Caen, France
[c] Normandie Univ, ENSICAEN, UNICAEN, CEA, CNRS, CIMAP
14000 Caen, France
[d] CEMCA UMR CNRS 6521
Université de Brest, IBSAM
6 Avenue Victor Le Gorgeu
29238 Brest, France
Supporting information for this article is available on the WWW under **http://dx.doi.org/10.1002/zaac.201600362** or from the author.

Results and Discussion

Structural Study

For the experimental conditions described below, needle shape crystals with an average length of 155 μm and width of 13 μm were isolated (Figure S1, Supporting Information). The single-crystal X-ray diffraction study of the phosphonate $Zn(H_2O)PO_3$–$C_{13}H_9$·H_2O shows that it crystallizes in the centrosymmetric space group $P2_1/c$ with the following parameters: a = 15.832(4) Å, b = 5.1915(10) Å, c = 17.519(4) Å, and

β = 114.479(6)° (Table 1) (for the atomic coordinates, the atomic displacement parameters, and the bond angles, see Supporting Information). All the hydrogen atoms could be located. In addition, the length of the four O–H bonds of the two water molecules was fixed at 0.85 Å. The projections of the structure along *b* (Figure 1) and along *c* (Figure 2) show that it consists of corner-shared $ZnO_3(H_2O)$ and PO_3C tetrahedra. One important structural feature of this compound deals with the one-dimensional character of the "Zn–P–O–C" framework, which forms $[Zn_2(PO_3)_2(H_2O)_2]_\infty$ tetrahedral chains parallel to the *b* axis and isolated from each other by the fluorene part of the ligand and by H_2O molecules (Figure 1). The second interesting feature concerns the fact that in those chains, the $ZnO_3(H_2O)$ tetrahedra are isolated from each other (Figure 2): each tetrahedron $ZnO_3(H_2O)$ has one free H_2O apex and shares its three other oxygen apices with three PO_3C groups. Thus the inorganic $[Zn_2(PO_3)_2(H_2O)_2]_\infty$ tetrahedral chains are separated by layers of conjugated organic fluorene ligands parallel to the (100) plane (Figure 2). The interatomic Zn–O distances, ranging from 1.912(3) Å to 2.007(3) Å, and P–O distances between 1.510(3) Å and 1.543(3) Å (Table 2), are in agreement with the data of the ionic radii given by *Shannon* and *Prewitt*.[26]

Table 1. Single crystal data of $Zn(H_2O)PO_3–C_{13}H_9·H_2O$ obtained at 150 K.

	$Zn(H_2O)PO_3–C_{13}H_9·H_2O$
Formula weight	345.57
Space group	$P2_1/c$
a /Å	15.832(4)
b /Å	5.1915(10)
c /Å	17.519(4)
α /°	90
β /°	114.479(6)
γ /°	90
Z	4
V /Å^3	1310.5(5)
d_{calc} /g·cm^{-3}	1.751
μ /mm^{-1}	2.011
Radiation source λ /Å	Mo-K_α 0.71073
Pattern range 2θ /°	5.11–56.62
No. of reflexions	3097
No. of soft constraints	4
wR (F^2) (weighted *R* factor)	0.1361
R [$F^2 > 2\sigma(F^2)$]	0.0509
R_{int} (internal *R* value)	0.0480
S (Goodness of the fit)	1.040

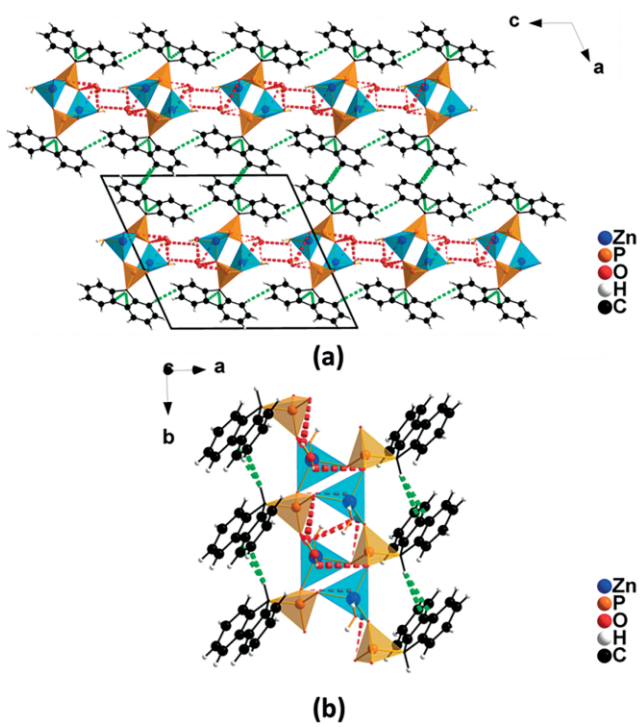

Figure 1. View of the structure of the zinc phosphonate $Zn(H_2O)PO_3–C_{13}H_9·H_2O$ along *b* axis (a) and representation of one of its columns along *c* axis (b). The $ZnO_3(H_2O)$ tetrahedra (blue colored) and the PO_3C tetrahedra (orange colored) form chains running along b. H_2O molecules (red) are intercalated between the chains. The red dashed lines represent the hydrogen bonds and the green dashed lines correspond to C–H···π bonds.

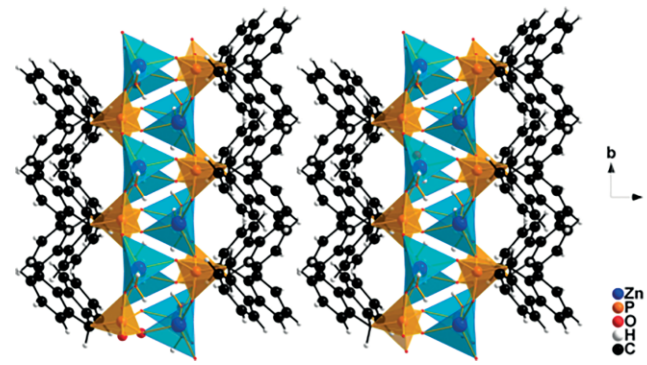

Figure 2. View of the structure of the zinc phosphonate $Zn(H_2O)PO_3C_{13}H_9·H_2O$ along *c* axis. The planar fluorenyl ligands (black) are oriented either parallel or perpendicular with respect to each other.

Table 2. Interatomic distances /Å for $Zn(H_2O)PO_3–C_{13}H_9·H_2O$.

Atom–Atom	Distance /Å	Atom–Atom	Distance /Å
Zn1–O3	1.912(3)	C4–C13	1.386(6)
Zn1–O1	1.925(3)	C4–C9	1.401(6)
Zn1–O2^{i}	1.961(3)	C4–H4	0.9500
Zn1–O4	2.007(3)	C5–C8	1.383(5)
P1–O3^{ii}	1.510(3)	C5–C14	1.393(6)
P1–O1	1.526(3)	C5–H5	0.9500
P1–O2	1.543(3)	C6–C10	1.405(5)
P1–C2	1.822(4)	C7–C12	1.378(6)
O5–H5A	0.833(19)	C7–C10	1.390(5)
O5–H5B	0.83(2)	C7–H7	0.9500
O4–H4A	0.8400	C8–C9	1.399(6)
O4–H4B	0.84(2)	C9–C10	1.464(5)
O3–P1^{iii}	1.510(3)	C11–C12	1.391(6)
C2–C8	1.512(5)	C11–H11	0.9500
C2–C6	1.516(5)	C12–H12	0.9500
C2–H2	1.0000	C13–C14	1.390(7)
C3–C6	1.381(5)	C13–H13	0.9500
C3–C11	1.397(6)	C14–H14	0.9500
C3–H3	0.9500	O2–Zn1^{i}	1.961(2)

(i) 1–*x*, 2–*y*, 1–*z*; (ii) *x*, –1+*y*, *z*; (iii) *x*, 1+*y*, *z*.

The organic conjugated fluorenyl ligands linked to the PO_3C tetrahedra play a crucial role in the stability of this structure since they ensure its cohesion in the directions perpendicular to

the zinc phosphonate columns, forming infinite double layers parallel to the (100) plane (Figure 2). One indeed observes strong C–H···π interactions between the organic ligands. This is illustrated by the fact that H···C bonds allow a two-dimensional network between the organic and inorganic parts (see green dashed lines in Figure 1a) to be formed, with H···C distances ranging from 2.70 Å to 2.90 Å. It must be noted that the C–H donor group belonging to PO_3C is bonded to the sp^3-hybridized carbon atom of the fluorenyl moiety. This C–H bond is located at a double benzylic position that likely explains its higher acidity and therefore its involvement in a hydrogen bond. Moreover hydrogen bonds between H_2O molecules and $ZnO_3(H_2O)$ tetrahedra, ranging from 2.70 Å to 3 Å (from O acceptor to H), are observed and are indicated as red dashed lines in Figure 1 which form additional links between the inorganic $[Zn_2(PO_3)_2(H_20)_2]_\infty$ tetrahedral chains in the (100) plane.

Hirshfeld Surface and Fingerprint Plot

In order to evaluate the importance of the C–H···π interactions with respect to other molecular bonds and to hydrogen bonds, a Hirshfeld Surface (HS)[27] analysis was performed using the program CrystalExplorer.[28] The latter characterizes the outer contour of the space occupied by the organic ligand in the crystal. Its comparison with the van der Waals envelope with which other ligands and molecules come into contact allows to evaluate the strength of interactions with those species. The mapping of these interactions can be made by means of various descriptors. In the presented case, shape index mapping (S) is best suited to observe subtle changes in the surface shape of the organic moiety of $Zn(H_2O)PO_3$–$C_{13}H_9$·H_2O such as complementary hollows (red) and bumps (blue) which are observed where two molecular surfaces touch one another (Figure 3a). The HS is shown as transparent in order to visualize the fluoren-9-yl $C_{13}H_9$ moiety. The presence of the pattern of red and blue triangles in the same area of the shape index surface (labeled 1 in the front and back view of the Figure 3a) is characteristic of π–π stacking. Besides, the C···H shape index mapping is best suited since C–H···π interactions play a major role in the stability of the structure. Indeed, the Figure 3b highlights large red and blue spots corresponding to C–H acceptor and donor interactions, respectively.

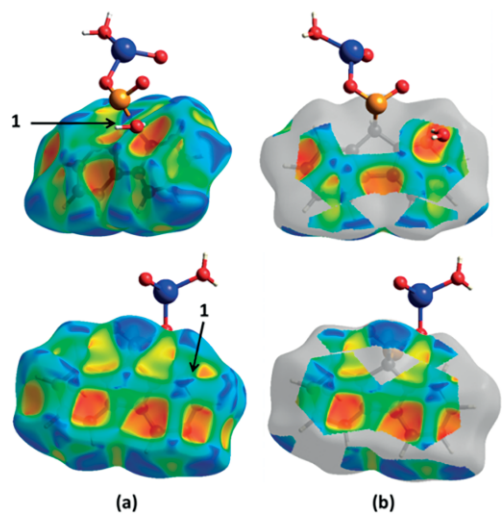

Figure 3. (a) Front (top) and back (bottom) view of the Hirshfeld surface (HS) represented on the fluorene part of $Zn(H_2O)PO_3$–$C_{13}H_9$·H_2O with shape index property mapped onto the surface. (b) Selective highlighting of C–H interactions represented on the shape index mode of the HS. Color code: –1.0 (concave umbilic; red) to 0.0 (minimal saddle; green) to +1.0 (convex umbilic; blue). Pictures are generated with the program *CrystalExplorer.*

The two-dimensional fingerprint plot[29] provides a brief summary of the intermolecular interactions and their relative area occurring in the fluorene part of $Zn(H_2O)PO_3$–$C_{13}H_9$·H_2O from d_i–d_e data point, i.e. points representing the distances from the surface to the nearest atom inside the molecule or to another molecule, respectively. The information of all percentage contributions of interactions of specific pairs of atom-types occurring in the Hirshfeld surface is given in Figure 4. The fingerprint plot matches with the previous expectations and shows a significant contribution of C···H contacts, which represent for a main part the C–H···π interactions (40.7 %) and H···H contacts (45.7 %). Concerning the O···H hydrogen bonds, they represent only 7.9 % and all other contact types (C···O, P···C, P···H) are less than 6 %. To have more details on the area of these contributions, the fingerprint plot is broken down into the different atom pair contacts in Figure S2 (Supporting Information).

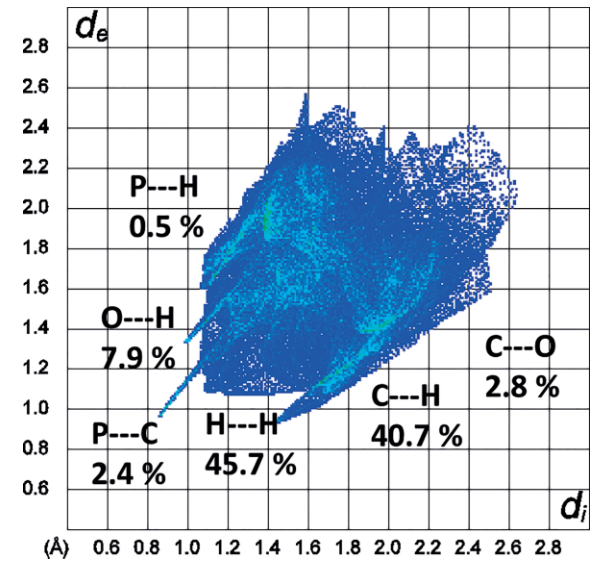

Figure 4. Two-dimensional fingerprint plot obtained with the program CrystalExplorer showing each contact type in the fluorene part of $Zn(H_2O)PO_3$–$C_{13}H_9$·H_2O with its overall percentage. d_i and d_e data points represent the distance from the surface to the nearest atom in the molecule itself or to another molecule, respectively.

Luminescence Properties

The UV/Vis absorbance spectrum of compounds fluoren-9-yl-phosphonic acid and $Zn(H_2O)PO_3$–$C_{13}H_9$·H_2O (Figure 5) shows absorption bands ranging from 261 to 311 nm and from 254 to 307 nm, respectively. Those distinct groups of absorption bands are attributed to $\pi \rightarrow \pi^*$ transitions originating from

states due to molecular short-axis and long-axis polarized states of the $C_{13}H_9$ ligand.[30,31] This similarity in absorption properties between fluoren-9-yl-phosphonic and $Zn(H_2O)PO_3$–$C_{13}H_9$·H_2O testifies to the fact that the mechanism of excitation of $Zn(H_2O)PO_3$–$C_{13}H_9$·H_2O is driven by its organic part. Considering the full $3d^{10}$ electronic configuration of Zn^{2+}, no electron can be promoted to a higher level by an excitation process with energy up to the visible, in agreement with the fact that Zn^{2+} alone does not present any absorption properties and produces usually a colorless or transparent material in the visible spectral range.[32] It has been shown previously that an electronic transition from the $3d^{10}4s^0(^2S_{1/2})$ level to the upper $3d^{10}4p^0(^2P_{1/2})$ state[33–35] can be considered. However, the latter would require an excitation energy superior to 6.0 eV (up to the far ultraviolet), which is much higher than the maximum excitation energy used in our spectroscopy experiments. Consequently the Zn^{II} remains in the ground state with full 3d sub-shell in all the spectroscopic experiment presented in this paper.

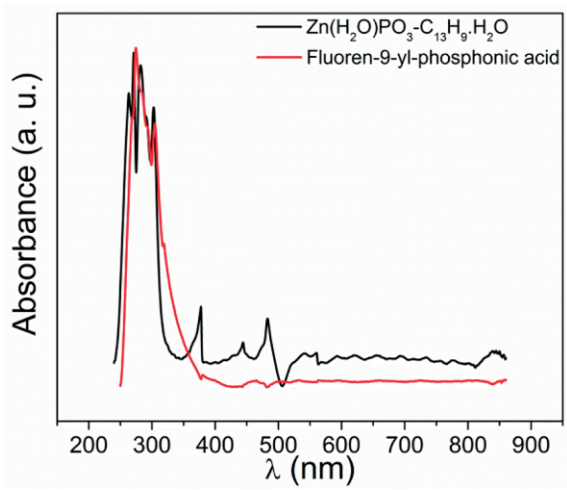

Figure 5. Normalized absorbance with baseline correction of $Zn(H_2O)PO_3$–$C_{13}H_9$·H_2O (black line) and fluoren-9-yl-phosphonic acid (red line) samples, obtained from specular transmittance measurement on powder.

The PL spectra of compounds fluoren-9-yl-phosphonic acid and $Zn(H_2O)PO_3$–$C_{13}H_9$·H_2O (Figure 6) show PL bands at 356, 419, and 552 nm and 359, 458, and 580 nm, respectively. Those distinct groups of emission bands are attributed to recombination occurring from π* excited states modulated by vibronic coupling. π-conjugated polymers have strong electron–phonon coupling and so, in addition to the π–π* emission, there is a manifold of vibronic overtones spaced approximately by about 100–200 meV apart and red-shifted from the dominant π–π emission band.[36] Thus, it appears clearly from the comparison of the two PL spectra that the conjugated fluorenyl ligands contribute to the absorption and emission properties of the fluorenylzinc phosphonate. The organic part of the molecule absorbs UV radiation, resulting in a π–π* transition to an excited state. The decay from this excited state may arise via a sequence of radiative and non-radiative mechanisms.

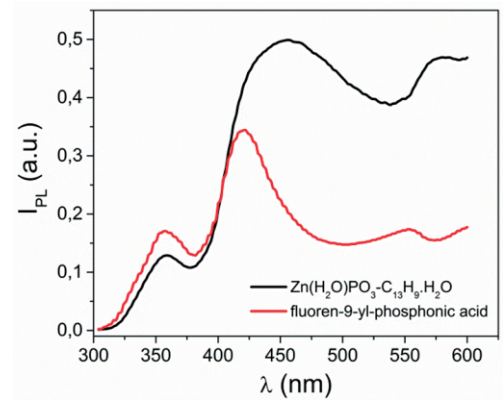

Figure 6. Photoluminescence spectra of $Zn(H_2O)PO_3$–$C_{13}H_9$·H_2O stacked between two quartz suprasil glass slides (black line) and of a fluoren-9-yl phosphonic acid single crystal (red line). Excitation line: 266 nm, power density of 23.5 mW·mm^{-2}, 900 gratings per mm, frequency of 9 Hz for $Zn(H_2O)PO_3$–$C_{13}H_9$·H_2O and 8.95 Hz for fluoren-9-yl phosphonic acid.

In order to understand the red shifting of the PL bands in this Zn phosphonate we have to consider the positions of the Zn^{2+} cation in the structure, i.e. the eventual bonds of this cation with the organic ligand which would allow ligand to metal charge transfer (LMCT) or metal to ligand charge transfer (MLCT) that are observed in zinc-organic complexes[2] and generate PL emission. In the present phosphonate Zn^{2+} ions are isolated from the ligands, i.e. are not linked to the latter (Figure 1 and Figure 2) and therefore are not contributing to LMCT/MLCT effects. Thus, it is most probable that zinc has a structural effect which favors particular orientations of the conjugated ligands. One indeed observes two types of arrangements of the latter, the slipped parallel and the 90° L-shaped configurations, which both exhibit strong C–H···π bonds characterized by short H···C distances of 2.79 Å. This Zn^{II} induces structural effect, which may contribute indirectly to the PL red shift by a modification of energy states of the organic part of the molecule participating in the sequence of radiative and non-radiative recombination.[31]

Conclusions

The fluorenyl conjugated ligand was introduced successfully in a zinc phosphonate, leading to a chain-like structure. This work demonstrates that the luminescence properties of this hybrid cannot originate from the isolated Zn^{2+} ion, but are due to the presence of strong C–H···π interactions. Thus, the red shift of the spectral bands with respect to the pure fluorenyl phosphonic acid originates from the structural constraints induced by the inorganic "Zn–P–O–C" chains.

Experimental Section

Synthesis: The zinc phosphonate $Zn(H_2O)PO_3$–$C_{13}H_9$·H_2O was synthesized from the fluoren-9-yl phosphonic acid and the zinc nitrate hexahydrate according to Scheme 1. For this hydrothermal synthesis, all reagents were used without prior purification. A polytetrafluoroeth-

ylene (PTFE) liner was charged with an equimolar mixture composed of zinc nitrate hexahydrate $Zn(NO_3)_2.6H_20$ (0.060 g, 0.203 mmol), fluoren-9-yl-phosphonic acid $C_{13}H_{11}O_3P$ (0.0501 g, 0.203 mmol) and urea $(NH_2)_2CO$ (0.0120 g, 0.203 mmol) dissolved in 15 mL of distilled water. The liner was inserted into a Berghof DAB-2 digestive vessel and heated from room temperature to 140 °C in 20 h, kept at this temperature for 30 h, and finally allowed to cool to room temperature within 20 h. The final product $Zn(H_2O)PO_3–C_{13}H_9·H_2O$, obtained as white needle-shaped single crystals, was filtered through Büchner, washed with distilled water, rinsed with ethanol, and finally dried in air. The chemical formula was confirmed by elemental analysis of carbon and hydrogen performed with ThermoQuest NA2500 setup: calcd.: C 45.2, H 3.8 %; found C 45.1(4), H 4.6(3) %

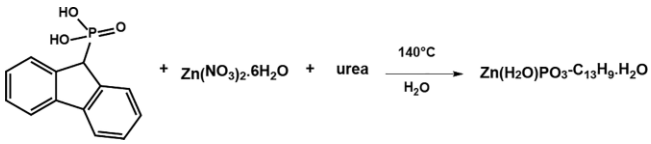

Scheme 1. Reaction of fluoren-9-yl phosphonic acid with zinc nitrate hexahydrate in urea medium.

Thermogravimetric Analysis: Thermogravimetric analysis was performed on a polycrystalline sample of $Zn(H_2O)PO_3–C_{13}H_9·H_2O$ under air atmosphere. The recorded curve (Figure S3, Supporting Information) shows that the weight loss below 250 °C (9.33 %) corresponds to the departure of the two water molecules (theoretical weight loss: 10.43 %). Beyond 290 °C, the next losses are due to the decomposition of the ligand and to the transformation at 900 °C of the dehydrated compound into zinc pyrophosphate $Zn_2P_2O_7$ (weight loss 54.62 %).

X-ray Diffraction and Structure Determination: A suitable single crystal was selected and X-ray diffraction experiment was performed at 150 K with a Bruker-Nonius Kappa CCD area detector diffractometer with graphite-monochromatized Mo-K_α radiation (λ = 0.71073 Å). Program used to solve structure: SHELXS-97.[37] Program used to refine structure: SHELXL-2014.[37] In order to check that the crystal is representative of the whole powder, a study by powder X-ray diffraction was performed. After analysis with the Fullprof software,[38] a simulation of the pattern was performed. All the peaks were indexed and were shown to match with space group $P2_1/c$ and lattice parameters found by single-crystal X-ray diffraction: a = 15.852 Å, b = 5.199 Å, c = 17.636 Å and β = 114.479° (see Figure S4, Supporting Information).

Crystallographic data (excluding structure factors) for the structure in this paper have been deposited with the Cambridge Crystallographic Data Centre, CCDC, 12 Union Road, Cambridge CB21EZ, UK. Copies of the data can be obtained free of charge on quoting the depository number CCDC-1505419 for $Zn(H_2O)PO_3–C_{13}H_9·H_2O$ (Fax: +44-1223-336-033; E-Mail: deposit@ccdc.cam.ac.uk, http://www.ccdc.cam.ac.uk).

Absorbance Spectra: Absorbance spectra were performed with a Perkin-Elmer lambda-1050 spectrophotometer in specular transmittance mode in normal incidence. Samples are constituted by powder of compounds stacked between two quartz Suprasil glass slides from Hellma Analytics.

Luminescence Spectra: Photoluminescence (PL) measurements were carried out at room temperature with a Crylas FQCW266 excitation laser emitting at 266 nm with an average power of 23.5 mW, with an incident angle of 45° on an area of about 1 mm^2 and chopped at 9.00 Hz for $Zn(H_2O)PO_3–C_{13}H_9·H_2O$ and at 8.95 Hz for fluoren-9-yl phosphonic acid. Emitted photons are collected into a light cone of 28° by means of a set of lens and a Horiba Jobin-Yvon Triax180 monochromator. The detection is ensured by R5108 Hamamatsu photomultiplier tube connected to a SR830 lock-in amplifer referenced at the excitation light chopper frequency. $Zn(H_2O)PO_3–C_{13}H_9·H_2O$ PL spectra was measured on powder stacked between two quartz suprasil glass slides from Hellma Analytics and fluoren-9-yl-phosphonic acid PL spectra was obtained on single crystal.

Supporting Information (see footnote on the first page of this article): scanning electron microscopy, fingerprint plots, thermogravimetry analysis and single crystal X-ray diffraction details.

Acknowledgements

We thank the Agence Nationale de la Recherche (contract N° ANR-14-CE07–0004–01 (HYMN)) for financial support. The authors also express their grateful acknowledgment for technical support to *Sylvie Collin* from the CRISMAT laboratory.

Keywords: Hybrid; Zinc; Phosphonate; Luminescence; Hirshfeld surface

References

[1] C. N. R. Rao, A. K. Cheetham, A. Thirumurugan, *J. Phys.: Condens. Matter.* **2008**, *20*, 083202.
[2] M. D. Allendorf, C. A. Bauer, R. K. Bhakta, R. J. T. Houk, *Chem. Soc. Rev.* **2009**, *38*, 1330–1352.
[3] S.-L. Zheng, J.-H. Yang, X.-L. Yu, X.-M. Chen, W.-T. Wong, *Inorg. Chem.* **2004**, *43*, 830–838.
[4] G. Alberti, U. Costantino, S. Allulli, N. Tomassini, *J. Inorg. Nucl. Chem.* **1978**, *40*, 1113–1117.
[5] S. Yamanaka, M. Tsujimoto, M. Tanaka, *J. Inorg. Nucl. Chem.* **1979**, *41*, 605–607.
[6] S. Yamanaka, M. Matsunaga, M. Hattori, *J. Inorg. Nucl. Chem.* **1981**, *43*, 1343–1346.
[7] A. Clearfield, K. D. Demadis, *Metal Phosphonate Chemistry: From Synthesis to Application*, RSC Publishing, London, **2012**.
[8] G. Alberti, U. Costantino, *Comprehensive Supramolecular Chemistry*, vol.7 (Eds.: J. L. Atwood, J. E. D. Davies, D. D. MacNicol, F. Vôgtle), Elsevier Science, New York, **1996**.
[9] K. Maeda, *Microporous Mesoporous Mater.* **2004**, *73*, 47–55.
[10] A. Clearfield, *Prog. Inorg. Chem.* **1998**, *47*, 371–510.
[11] N. Hugot, M. Roger, J. M. Rueff, J. Cardin, O. Perez, V. Caignaert, B. Raveau, G. Rogez, P. A. Jaffrès, *Eur. J. Inorg. Chem.* **2016**, *2*, 266–271.
[12] S.-M. Ying, J.-G. Mao, *Cryst. Growth Des.* **2006**, *6*, 964–968.
[13] K. J. Gagnon, H. P. Perry, A. Clearfield, *Chem. Rev.* **2012**, *112*, 1034–1054.
[14] R. Luebeke, L. J. Weselinski, Y. Belmabkhout, Z. Chen, L. Wojtas, M. Eddaoudi, *Cryst. Growth Des.* **2014**, *14*, 414–418.
[15] M. Berchel, T. Le Gall, C. Denis, S. Le Hir, F. Quentel, C. Elléouet, T. Montier, J. M. Rueff, J. Y. Salaün, J. P. Haelters, P. Lehn, G. B. Hix, P. A. Jaffrès, *New J. Chem.* **2011**, *35*, 1000–1003.
[16] J. M. Rueff, V. Caignaert, S. Chausson, A. Leclaire, C. Simon, O. Perez, L. le Pluart, P. A. Jaffrès, *Eur. J. Inorg. Chem.* **2008**, 4117–4125.
[17] W. Dan, X. Liu, M. Deng, Y. Ling, Z. Chen, Y. Zhou, *Inorg. Chem. Commun.* **2013**, *37*, 93–96.
[18] C. Heering, B. Francis, B. Nateghi, G. Makhloufi, S. Lüdeke, C. Janiak, *CrystEngComm* **2016**, *18*, 5209–5223.

[19] R. Fu, S. Hu, X. Wu, *Cryst. Growth Des.* **2015**, *15*, 5021–5027.
[20] F. Tong, Z.-G. Sun, K. Chen, Y.-Y. Zhu, W.-N. Wang, C.-Q. Jiao, C.-L. Wang, C. Li, *Dalton Trans.* **2011**, *40*, 5059–5065.
[21] a) R. Fu, S. Hu, X. Wu, *CrystEngComm* **2013**, *15*, 8937–8940; b) R. Fu, S. Hu, X. Wu, *J. Solid State Chem.* **2011**, *184*, 945–952; c) H. He, P. Zhang, Y. Ling, Z. Chen, Y. Zhou, *ChemPlusChem.* **2016**, *81*, 822–827.
[22] X. Li, Y. Sun, Y. Chen, Z. Zhou, Z. Du, *Struct. Chem.* **2012**, *23*, 91–96.
[23] Y.-S. Ma, X.-Y. Tang, W.-Y. Yin, B. Wu, F.-F. Xue, R.-X. Yuan, S. Roy, *Dalton Trans.* **2012**, *41*, 2340–2345.
[24] R. Singleton, J. Bye, J. Dyson, G. Baker, R. M. Ranson, G. B. Hix, *Dalton Trans.* **2010**, *39*, 6024–6030.
[25] G. B. Hix, V. Caignaert, J. M. Rueff, L. Le Pluart, J. E. Warren, P. A. Jaffrès, *Cryst. Growth Des.* **2007**, *7*, 208–211.
[26] R. D. Shannon, C. T. Prewitt, *Acta Crystallogr., Sect. B* **1969**, *25*, 925–946.
[27] a) M. A. Spackman, D. Jayatilaka, *CrystEngComm* **2009**, *11*, 19–32; b) J. J. McKinnon, M. A. Spackman, A. S. Mitchell, *Acta Crystallogr., Sect. B* **2004**, *60*, 627–668.
[28] S. K. Wolff, D. J. Grimwood, J. J. McKinnon, M. J. Turner, D. Jayatilaka, M. A. Spackman, University of Western Australia, **2012**.
[29] M. A. Spackman, J. J. McKinnon, *CrystEngComm* **2002**, *4*,378–392.
[30] F. C. Correia Santos, T. C. F. Santos, J. R. Garcia, L. O. Peres, S. H. Wang, *J. Braz. Chem. Soc.* **2015**, *26*, 84–91.
[31] T. G. Pavlopoulos, *Spectrochim. Acta Part A* **1986**, *42*, 1307–1310.
[32] N. M. Avram, M. G. Brik, *Optical Properties of 3d-Ions in Crystals: Spectroscopy and Crystal Field Analysis*, Springer Science & Business Media, Heidelberg, **2013**.
[33] D. Gullberg, U. Litzén, *Phys. Scripta* **2000**, *61*, 652–656.
[34] W. C. Martin, V. Kaufman, *J. Res. Natl. Bur. Stand.* **1970**, *74*, 11–22.
[35] J. Sugar, A. Musgrove, *J. Phys. Chem. Ref. Data.* **1995**, *24*, 1803–1872.
[36] M. Knaapila, M. J. Winokur, *Adv. Polym. Sci.* **2008**, *212*, 227–272.
[37] G. M. Sheldrick, *Acta Crystallogr., Sect. C* **2015**, *71*, 3–8.
[38] J. Rodriguez-Carvajal, *Phys. B* **1993**, *192*, 55.